# Oceanic Rain Identification using Multi-Fractal Analysis of QuikSCAT Sigma-0

**Vasud Torsekar, Takis Kasparis, W. Linwood Jones and Khalil Ahmad**
Central Florida Remote Sensing Laboratory
University of Central Florida, Orlando, FL 32826

**David G. Long**
Microwave Earth Remote Sensing Laboaratory
Brigham Young University, Provo, Utah 84602

*Abstract –* **The presence of rain over oceans interferes with the measurement of sea surface wind speed and direction from the SeaWinds scatterometer, and as a result, in rain regions wind measurements contain biases. In past research at the Central Florida Remote Sensing Lab, it has been observed that rain has multi-fractal behavior. In this paper we present an algorithm to detect the presence of rain so that rain regions are flagged. The forward and aft views of the high resolution horizontal polarization backscatter are used for the extraction of textural information with the help of multi-fractals. A negated multi-fractal exponent is computed to discriminate between wind and rain. Pixels with exponent value above a threshold are classified as rain pixels and those that do not meet the threshold are further examined with the help of correlation of the multi-fractal exponent within a predefined neighborhood of individual pixels. It was observed that the rain has less correlation within a neighborhood compared to wind. This property is utilized for reactivation of the pixels that fall below a certain threshold of correlation. An adaptive multifractal exponent and threshold is used, as we deal with a wide range of latitudes. Validation results are presented through comparison with the Tropical Rainfall Measurement Mission Microwave Imager (TMI) 2A12 rain retrieval product for one day. The results show that the algorithm is effective in identifying rain pixels. Some algorithm deficiencies in high wind speed regions are also discussed. Comparisons with other proposed approaches are also be presented.**

## I. INTRODUCTION

**QuikSCAT** is a Ku-band satellite launched for the global mapping of ocean surface vector winds. The **SeaWinds** instrument on the QuikSCAT satellite is specifically designed to make high-precision measurements of the normalized radar cross-section ($\sigma_0$) of the ocean surface. Since ocean surface roughness is very sensitive to the surface wind velocity, $\sigma_0$ can be used to estimate the ocean surface wind velocity. The ocean winds are estimated via an empirically determined relationship between $\sigma_0$ of the ocean and the wind vector. This relationship is called the **Geophysical Model Function (GMF)** [1], [2]. However the Ku-band scatterometers' performance degrades for precipitating and extremely high wind conditions.

Specifically, rain has 3 effects on scatterometer measurement,
1) It attenuates the scatterometer signal,
2) It introduces volume scattering by rain-drops and
3) It perturbs the water surface and consequently, influences the backscatter from the surface.

These effects of rain on QuikSCAT were found to be severe for low and moderate wind speeds (<10 m/s) [3]. If the Geophysical Model Function (GMF) does not incorporate these effects, the rain attenuation and backscatter are interpreted as wind-induced features. The additional scattering from rain causes the estimated wind speeds to appear higher than expected. This can be referred to as the 'overestimation of wind speed'. Also the directions of the rain-corrupted wind vectors generally point cross-swath, regardless of the true wind direction.

QuikSCAT is particularly more susceptible to rain corruption than previous scatterometers, due to its relatively large incidence angles [4]. Higher incidence angles lead to greater scattering and attenuation from the rain column. To prevent the meaningless values and over-estimation of wind velocity, it is necessary to flag the rain-affected regions in the $\sigma_0$ map.

Many approaches have been devised in the past to tackle this problem. Stiles et. al. [3] tried to model the impact of rain on Ku-band wind scatterometer data employing collocated QuikSCAT $\sigma_0$, SSM/I rain-rate measurements, and NCEP wind-fields to empirically fit a simple theoretical model. Long et. al. [5] used a simple backscatter model with collocated Precipitation Radar data from TRMM satellite to evaluate the effect of rain on collocated data to find optimum parameters for their empirical fit. This model was used to simultaneously retrieve wind and rain [6], which can be used as a rain flag. Weissman et. al. [4] have utilized a basic property of $\sigma_0$ in the rain-affected regions. They found that the H-pol $\sigma_0$ exceeds the V-pol $\sigma_0$ in the rain-affected regions. The difference between these 2 polarizations $\sigma_0$ is termed as the "Differential Reflectivity". This differential $\sigma_0$ along with the R-Z relationship is used to retrieve rain-rates from $\sigma_0$.

Multifractals have been used in the past for interpreting meteorological data. Some previous techniques examine the multifractal behavior of rainfall in both temporal and spatial domain[7], [8]. In the past research at the Central Florida Remote Sensing Laboratory at University of Central Florida, multifractal nature of precipitation was used for quality control of the NEXRAD data [9]. In this paper we have used multifractals to extract the textural information from the forward and aft views of the high-resolution H-pol $\sigma_0$. A negated multifractal exponent is computed to discriminate beween wind and rain. Pixels with exponent value above a certain threshold are classified as rain pixels and those that do not meet the threshold are further examined with the help of correlation of the multifractal exponent within a predefined neighborhood of individual pixels before and after the threshold is applied. Rain has less correlation than

wind. This property was utilized for reactivation of pixels that fell below a certain threshold of correlation. The multifractal exponent and the threshold are set adaptively depending on the average intensity found in a predefined surrounding region of a pixel.

To validate our results we used Tropical Rainfall Measurement Mission Microwave Imager (TMI) 2A12 rain retrieval products for one day. We have also compared our method with the differential reflectivity approach proposed by Weissman et. al. in [4].

The paper is organized as follows. Section II reviews the viewing geometry of QuikSCAT satellite and the high resolution $\sigma_0$ we used in this project. A brief introduction to the multifractal theory is presented in section III. Section IV describes the Rain Detection algorithm in detail.The results and conclusions are presented in section V and the summary in section VI.

## II. QuikSCAT viewing geometry and High Resolution SIR data.

### A. QuikSCAT Viewing Geometry

The SeaWinds instrument on QuikSCAT is a pencil-beam scanning scatterometer collecting $\sigma_0$ measurements at 13.4 GHz. The QuikSCAT satellite revolves in a near polar orbit and covers over 90% of the earth daily. It differs from the previous fan-beam scatterometer designs in that instead of multiple wide-beam stationary antennas, it has a conical scanning parabolic antenna illuminated by 2 feeds. The 2 feeds are used to transmit 2 beams of differing incidence angles and polarizations, producing 2 helices of measurements upon the ground, as the spacecraft moves along its track. The inner beam is horizontal polarization (H-pol) incidence. The outer is vertical polarization (V-pol) at $54^0$. Each 25 km X 25 km ground cell is sampled 8-15 times.However these samples are not distributed uniformly in azimuth but rather correspond to four disjoint narrow ranges of azimuth angles from forward and aft half of the antenna rotation and from each beam. These four look-sets are relevant for wind-direction discrimination. As seen later, we have used 2 look-sets out of the four, for the purpose of rain-detection. Fig. 1 shows the QuikSCAT viewing geometry. For simplicity circles are used to depict each scan. A circle is a good approximation for a single rotation of the antenna, as the 'gap' in the beam ground track which results from movement of the spacecraft is only 25 km as compared to 700 km for the radius of the inner beam scan [3].

### B. High Resolution SIR data

Space-borne scatterometers are satellite instruments that were originally designed to map wind-speed and direction over oceans, but they also measure various land and ocean variables. Scatterometer actively transmit electromagnetic pulses to the earth's surface and measure the backscatter response, or the power of the returned pulse scattered back to the antenna. While originally designed for wind observation, scatterometers have proven useful in a variety of land and ice studies. To further improve the utility of the data, resolution enhancement algorithms have been developed. These algorithms produce images of the surface $\sigma_0$ at enhanced resolution (to better than 10 km). Both conventional and enhanced resolution products are included in the SIR product suite [10], [11]. The enhanced resolution products are produced with the aid of **Scatterometer Image**
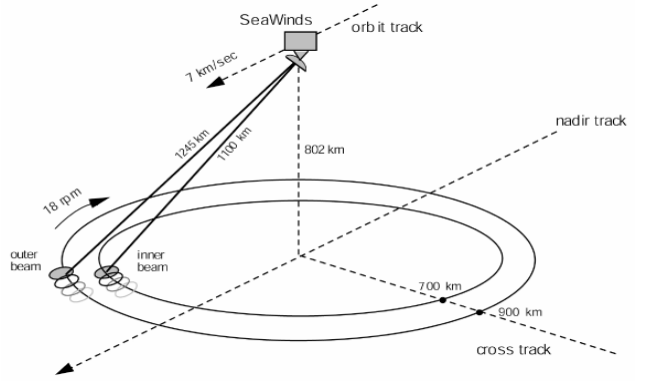
**Reconstruction (SIR) Algorithm** in [10].



Fig. 1. QuikSCAT viewing geometry

The **SIR** algorithm is based on a multi-variate form of a block multiplicative algebraic reconstruction. Combining multiple passes and robust performances in the presence of noise, it provides enhanced resolution measurements of the surface characteristics. Following is an intuitive explanation of the SIR algorithm.

Let $f(x, y)$ be a function that gives $\sigma_0$ at a point $(x, y)$. The scatterometer measurement system can be modeled by,

$$Z = Hf + noise \qquad (1)$$

where, $H$ is an operator that models the measurement system (sample spacing and aperture filtering) and $Z$ repressnts measurements of $\sigma_0$ made by the instrument sensor. The set of measurements $Z$ are discrete sampling of the function convolved with the aperture function.

Resolution engnacement is an inverse problem.

$$\hat{f} = \hat{H}^{-1} z$$

(2)

where, $\hat{f}$ is an estimate of $f$ from the measurements $z$. The inverse of the operator $H$, $H^{-1}$ is exact only, if $H$ is invertible and the measurements are noise-free, in which case $\hat{f} = f$. This represents a form of resolution enhancement, since informaton in the sidelobes of the measurement response or aperture function is recovered in the inversion, producing images at a finer resolution that the original measurements. In effect, the SIR algorithm is an inverse reconstruction filter optimized to minimize noise in the scatterometer reconstructed image.

Unlike NSCAT, which made $\sigma_0$ measurements over a broad range of incidence angles, QuikSCAT makes $\sigma_0$ measurements at only 2 nominal incidence angles $46^0$ and $54.1^0$, corresponding to the inner and outer beams. The inner beam measurement is H-pol while the outer beam is V-pol. Since it is undesirable to combine measurements from different polarizations, a single-variate form of SIR similar to the type developed for radiometer applications is used to generate enhanced resolution images of $\sigma_0$ at each of the 2 polarizations.

### III. Multi-Fractal Theory

Multifractals have been found to be very useful in the

analysis of complex geophysical systems. They are based on the principle of scale-invariance. Scale-invariance analysis is a framework for developing statistical tools that account for all available scales at once. Scale-invariance is a property that is respected by systems, whose large and small scales are related by a scale changing operation involving the scale-ratio.This leads to the fact that these systems do not have a characteristic scale. In multifractal analysis a power-law behavior is sought for, of a partition function that is constructed from a measure, with respect to the scale-parameter under consideration. If a single power-law exponent is sufficient to characterize all statistics within a whole family, then we refer to the model as monofractal. If more than one exponent is needed to characterize the statistical behavior of the signal, then we refer to the model as multifractal.

As we mentioned before, the scaling behavior of signals can be expressed by different scale-independent relationships. Scale $s$ can be defined as a parameter that specifies the size of the area under consideration. Assume that the random process studied is an $N$-dimensional signal $f(x_1, x_2, .....x_N)$. The goal in multi-fractal analysis is the examination of the different statistical characteristics of the signal $f$. For that purpose, a statistical measure $\mu_q$ is extracted from the function $f$. The measure $\mu_q(s, x_1, x_2, .....x_N)$ at scale s at the location $(x_1, x_2, .....x_N)$ of the N-dimensional signal is defined as,

$$\mu_q(s, x_1, x_2, .....x_N) = \varepsilon_s^q(s, x_1, x_2, .....x_N) \qquad (3)$$

Where,

$$\varepsilon_s(s, x_1, x_2, ......x_N) = \sum_{x_1'=x_1-s/2}^{x_1+s/2} \sum_{x_N'=x_N-s/2}^{x_N+s/2} f(x_1', x_2'..., x_N') \qquad (4)$$

is the sum of the function $f$ inside a box of size $s \times s \times ......\times s$ . The scale-dependent $q^{th}$ moment ensemble average of the measure $\mu_q(s, x_1, x_2, .....x_N)$ is called the partition function $<\varepsilon_s^q>$ . Basically the partition function at the point with coordinates $(x_1, x_2, .....x_N)$ is the $q^{th}$ moment of the function $f$, around point $(x_1, x_2, .....x_N)$, at scale $s$. The scale dependent statistical behaviour of the function $f$ at point $(x_1, x_2, .....x_N)$ can be examined by the change of the statistical moments, computed around $(x_1, x_2, .....x_N)$, from one scale to another. Then, one looks for a power-law relation between the partition functions (scale-dependent moments) and the scale parameter under consideration that describes the variation if the statistical moments with scale $s$. In our analysis the function $f$ is defined on a discrete domain, since it is samples version of the continuous function. Then the power-law relation is defined as,

$$\langle \varepsilon_s^q \rangle \square \ s^{K(q)} \qquad (5)$$

The function $K(q)$ is the so called '**moment scaling function**' and characterizes the multi-fractal behaviorof the signal $f$. If the function, $K(q)$ is a straight line then a single power-law exponent is sufficient to characterize all statistics within a whole family and then its called monofractality. If the function $K(q)$ is not a straight line then more than one exponent is needed to charactetize the

statistical behavior of the signal and then it is called as multifractality. Practically the ensemble average $<\varepsilon_s^q>$ is approximated by the spatial average of $\varepsilon_s^q$ under assumption of temporal stationarity of the function $f$. If we consider applying the log at both sides of (5), then the function $K(q)$ is estimated from the slope of the line that best fits the points $(log \ s, \ log <\varepsilon_s^q>)$ at $s = s_1, s_2,....s_L$ ,where $s_1$ is the smallest availabel scale and $s_L$ is the largest available scale.

## IV. Rain Detection Algorithm

The rain detection algorithm uses the forward and aft views of the high resolution H-pol and V-pol $\sigma_0$ . We had four flavors of the high resolution QuikSCAT data available, but we chose the horizonatal polarization pair, because horizontal polarization has better contrast than that of vertical polarization.

*A. Pre-processing:*

Before we actually analyse the data with multifractals and correlation, we bring it into desired format. The high-resolution data we deal with had 15 passes of QuikSCAT $\sigma_0$ for one day. Each pass consists of $760 \times 16231$ data points, with 16231 corresponding to latitudes and 760 corresponding to the longitudes. The data was not earth- gridded. Due to the polar orbit of QuikSCAT, each pass covered almost entire range of latitudes, from $-90^0$ to $+90^0$. We have considered only tropical regions extending from latitudes of $-40^0$ to $+40^0$, as in TRMM validation data, for the purpose of comparison. Even though this reduces the latitude range, it is still wide and the weather undergoes tremendous changes along this wide latitude range. Thus, it is not reasonable to use one single global exponent and threshold. We have used an adaptive exponent and threshold to take into consideration the wide latitude range. The 2 variables, exponent and threshold are adapted depending on the average intensities in a predefined neighborhood. We fixed this neighborhood to 500 pixels along the latitudes. The value ,500 pixels, was empirically determined by comparing the results at many different neighborhood sizes ranging from 700 to 300 pixels along the latitudes. Thus, we divided each pass into 17, $760 \times 500$ pixel images and then processed them one by one.

We used two properties of rain and wind echoes for separation. The first property is that rain echoes have higher multifractal exponent than the wind echoes. The second property is that wind echoes have higher correlation in comparitively larger neighborhoods than rain echoes.

*B. Step 1. Use of multifractal exponent for the description of texture.:*

We have used the forward and aft views of high resolution $\sigma_0$. The signal is considered to be a three dimensional signal. We assume that the scale s takes two values namely, $s_1$ and $s_2$. We define the measure at the scale $s_1$ as:

$$\mu_q(s_1, x, y, z) = [f(x, y, z)]^q \qquad (6)$$

The measure at scale $s_2$ is defined as:

$$\mu_q(s_2,x,y) = \left[ \sum_{x'=x-1}^{x+1} \sum_{y'=y-1}^{y+1} \sum_{z'=1}^{2} f(x',y',z') \right]^q \quad (7)$$

The coordinates *(x,y,z)* correspond to the pixel that exists in the *(x,y)* position of the forward or the aft view. The power-law is the same as in eqn.(5). The function *K(q)* is estimated from the slope of the line that best fits the points (*log s, log* $< \varepsilon_s^q >$ ) at $s = s_1, s_2$ . The function *K(q)* is then equal to

$$\frac{\log\left\langle \varepsilon_{s_2}^q \right\rangle - \log\left\langle \varepsilon_{s_1}^q \right\rangle}{\log(s_2) - \log(s_1)}$$

(8)

The ensemble average in (8) is approximated with the spatial average of the measures in small 3-D windows

$$\left\langle \varepsilon_{s_2}^q \right\rangle \Big|_{x,y}^w = (1/2w^2) \sum_{x'=x-w/2}^{x+w/2} \sum_{y'=y-w/2}^{y+w/2} \sum_{z'=1}^{2} \mu_q(s_2,x',y',z')$$

(9)

$$\left\langle \varepsilon_{s_1}^q \right\rangle \Big|_{x,y}^w = (1/w^2) \sum_{x'=x-w/2}^{x+w/2} \sum_{y'=y-w/2}^{y+w/2} \mu_q(s_2,x',y')$$

(10)

From (8), (9), and (10), $K_{x,y}^w(q)$ are calculated. W denotes the local neighborhood in which the measures are averaged. Thus, different multifractal exponents can be computed using different exponents (q) and also the local window sizes (w). The exponent and window size that can be used in a particular region depends on the average intensity in that particular region.

To obtain optimum results we have used adaptive value of "q". We defined various average intensity regimes and for each regime we found the optimum exponent value q. After the multifractal exponent is calculated, it is thresholded to separate rain events that are very obvious. The threshold used at this stage is also adaptive, for the same reason, as the exponent. We have also found the optimum threshold level for the different average intensity regimes mentioned before. The various average intensity regimes and the corresponding exponent and the threshold levels are summarized in Table 1.

*C. Step 2.Computation of Correlation of the Multifractal exponent within a predefined neighborhood:*
After thresholding we find the correlation of the multifractal exponent image in a predefined neighborhood

TABLE 1
AVERAGE INTENSITY REGIMES AND ADAPTIVE VALUES OF q
AND THRESHOLD

| Average Intensity Regime | Exponent (q) | Threshold |
|---|---|---|
| $m \le 70$ | 5.5 | 61 |
| $70 < m \le 90$ | 6.0 | 61 |
| $90 < m \le 105$ | 6.5 | 65 |
| $105 < m \le 135$ | 7.0 | 65 |
| $m > 135$ | 7.5 | 75 |

We have used a window-size of $25 \times 25$ for this purpose. We find two types of correlations. The first correlation excludes all the pixels that were removed in the first step in the process of thresholding, while the second correlation includes the pixels that were removed in the first step. The objective at this stage is to reactivate all the pixels that were removed in the first step because of the strict thresholds. There are twotypes of such pixels,
1. The pixels that lie at the boundaries of the prominent rain events. These pixels have intensities lower than the central part of the event and get erased.
2. The pixels that correspond to very weak rain events, which are removed due to the strict thresholds in the first step.

The first type of pixels mentioned above are reactivated by comparing the 2 correlations. If the value of correlation changes for a pixel, it is reactivated. The second type of pixels are activated by thresholding the second correlation. This step utilizes the property of the rain events that rain has lower correlation that wind pixels in a relatively larger neighborhood. This neighborhood is fixed at $25 \times 25$ as mentioned before.

*D. Step 3 Application of a noise threshold to remove the artifacts:* The thresholding applied in the previous steps produces artifacts. To get rid of these artifacts we apply a nominal noise threshold of intenisty 20.

*E. Post-processing:*
After all 15 passes were processed, we combined all the passes and earth-gridded them to be able to compare them with the validation results.

V. Results

We discuss the results in 3 subsections. In the beginning we discuss the comparison of our results with the validation data. In the second subsection we discuss some deficiencies of our algorithm in regions with very strong winds. Finally, in the third subsection we compare multi-fractal rain-flag with the differential reflectivity rain-flag from [4].

*A. Comparison with the validation TRMM data:*
We processed one day (Julian day 315, 10th Nov 2004) of QuikSCAT high resolution H-pol aft and forward $\sigma_0$. The results were validated with TRMM TMI rainrates.It should be noted that the comparison with TRMM is intended only to validate the presence of rain and not the comparison of the actual rain-rates.

Multiple passes were earth-gridded and averaged to match the TRMM resolution of $0.25^0$ of latitude and longitude. The comparisons are not necessarily at co-locations. This is so, because we did not find many co-locations, with precipitation. Fig. 2 to 9 show the comparisons of the QuikSCAT rain flag with TRMM rain rate. The rain-affected pixels have been identified clearly in the QuikSCAT images. Although the intensities of the individual pixels do not match that of the validation TRMM data, the rain-detection algorithm has been able to identify the rain-affected pixels.

*B. Deficiencies in strong wind regions :*
The rain-detection algorithm some times tends to

4

produce false alarms in regions with winds over 20-25 m/s. There are 2 apparent reasons for the false alarms. The algorithm utilizes the local information around a pixel in the form of the average intensity to find the optimum parameters for the neighborhood. Even though average intensity is a satisfactory measure to evaluate the local characteristics, it some times can give misleading interpretations. When a region contains very high as well as very low winds, the average intensity in such regions is not very high. But still these regions have strong wind regions within them. Such values of average intensities do not represent the neighborhood correctly. Because of this the algorithm selects parameters that are lower than the required value and produce false alarms. The second possible reason for false alarms is the rain events that are surrounded or accompanied by very strong winds. In such events the algorithm tends to reactivate the wind pixels as they are very close to or on the boundary of the rain event Fig.10 to 13 show these regions with high wind. The validation data we used for this purpose was taken from Remote Sensing Syestems, QuikSCAT wind retrieval [12].

*C. Comparison of multifractal rain-flag with differential polarization rain-flag :*

We have compared our results with another approach proposed by Weissman et. al. in [4]. The differential reflectivity is utilized to flag rain-affected pixels in [4]. We generated rain-flags using differential reflectivity with our data for the purpose of comparisons. Differential reflectivity technique produces somewhat noisier rain-flags in the regions with strong wind compared to the rain-flags generated with multi-fractals. Differential polarization also produces false alarms in many regions, which are not necessarily strong wind regions. There are also some regions where differential polarization fails to identify rain pixels. The comparisons of differential polarization and multifractal rain flags are shown in Fig. 14 to 17.

## VI. Summary

A rain detection algorithm has been developed using multifractal analysis and correlational behavior of rain echoes. The algorithm does not require any training. It works with fixed parameters. The results obtained were validated using TRMM TMI 2A12 data. Algorithm works very well in presence of moderate and high winds. False alarms are observed in presence of strong winds.

### Acknowledgment

## REFERENCES

[1] C. Y. Chi, F. K. Li, " A comparitive study of several wind estimation algorithms of spaceborne scatterometers," *IEEE Trans Geosc and Rem. Sens.,* vol. 26, No. 2, pp. 115-121, Mar. 1988.

[2] M. H. Frielich, R. S. Dunbar, " Derivation of Satellite Wind Model Functions Using Operational Surface Wind Analyses: An Altimeter Example," *J. of Geophys. Res.,* vol. 98, No.V8, pp. 1463-14649, Aug.1993

[3] B. W. Stiles, S. Yueh, "Impact of Rain on Spaceborne Ku-Band Wind Scatterometer Data", *IEEE Trans Geosc and Rem. Sens.,* vol. 40, No.9, pp. 1973-1983, Sept. 2002.

[4] D. E. Weissman, M. A. Bourassa, J. J. O' Brien, J. S. Tongue, "Calibrating the QuikSCAT/SeaWinds Radar for Measuring Rainrate Over the Oceans", *IEEE Trans Geosc and Rem. Sens.,* vol. 41, No.12, pp. 2814-2820, Dec. 2003

[5] D. W. Draper, D. G. Long, "Evaluating the effect of rain on SeaWindsscatterometer measurements," *J. of Geophys. Res..,* vol. 109, No.C02005, Feb. 2004.

[6] D. W. Draper and D. G. Long, "Simultaneous Wind and Rain Retrieval Using SeaWinds Data," *IEEE Trasn Geosc and Rem Sens,* vol. 42, no. 7, pp. 1411-1423, 2004.

[7] M. Alber,J.Peinke,"Improved multifractal box-counting algorithm, virtual phase transitions, and negative dimensions", *Phys. Rev. Let. E,*vol. 57, No. 5, pp. 5489-5493, May 1998

[8] M. I. P. de Lima, J. Grasman, "Multifractal Analysis of 15-min and daily rainfall from semi-arid region in portugal," *J. of Hydrology*, vol. 220, , April 1999

[9] D. Charalampidis, T. Kasparis, W.L. Jones, "Removal of Non-precipitation Echoes in Weather Radar Using Multi-fractals and Intenisity," *IEEE Trans Geosc and Rem. Sens.,* vol. 40, No.5, pp. 1121-1131, May 2002.

[10]D. G. Long, "Standard BYU QuikSCAT/SeaWinds Land/Ice Products," *Microwave Earth Remote Sensing Laboratory, BYU, Provo, Utah 84602, http://www.scp.byu.edu/*

[11]D. S. Early and D. G. Long, "Image Reconstruction and Enhanced Resolution Imaing from Irregular Samples," *IEEE Trans Geosc and Rem Sens.,*vol. 39, no. 2, pp. 291-302, 2001.

[12] Web-Source, Remote Sensing Systems Website, QuikSCATwind-retrieval, *http://www.remss.com*
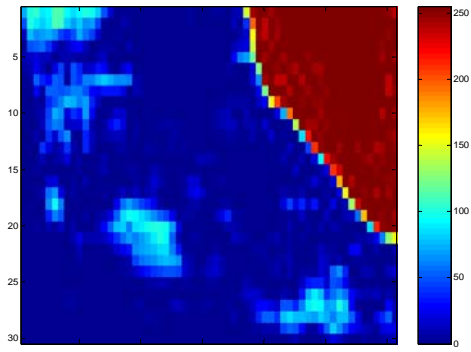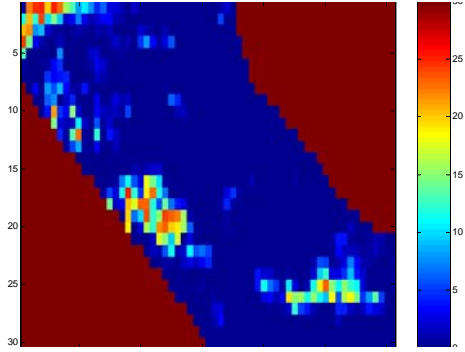
Fig 2 QuikSCAT Rain-flag
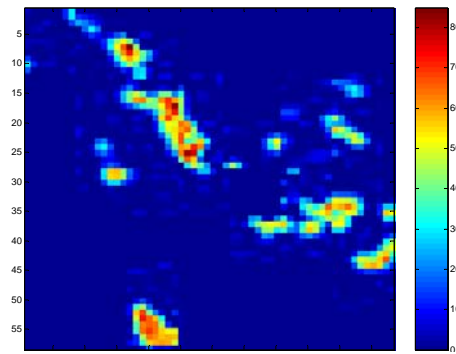


Fig 3   TRMM rain-rate
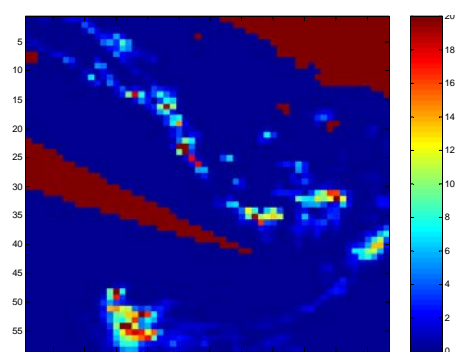


Fig 4 QuikSCAT Rain-flag
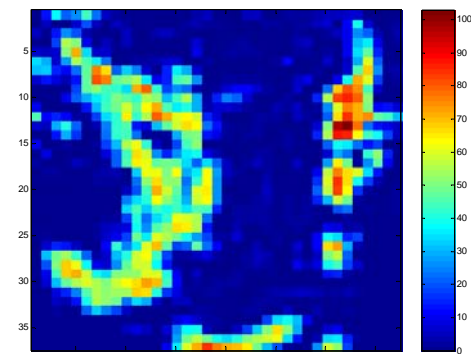


Fig 5   TRMM rain-rate
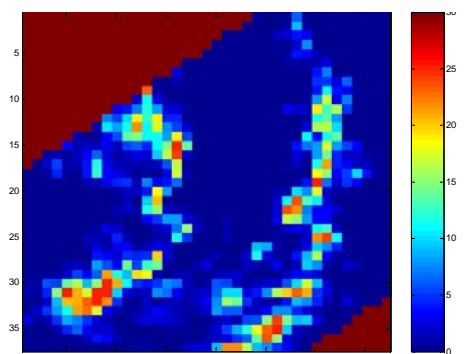


Fig 6 QuikSCAT Rain-flag


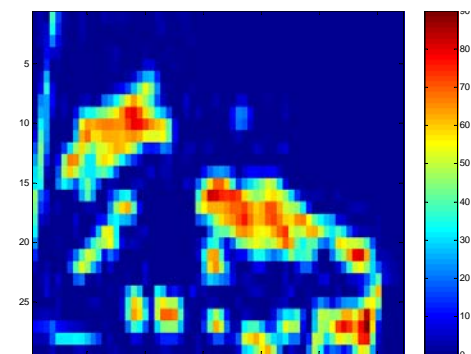
Fig 7   TRMM rain-rate



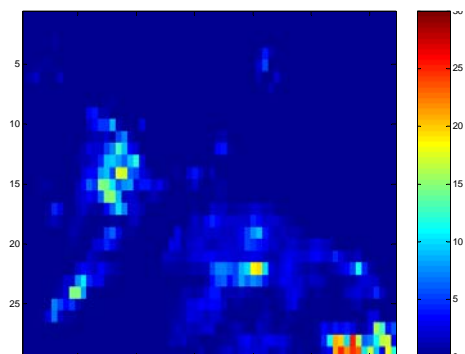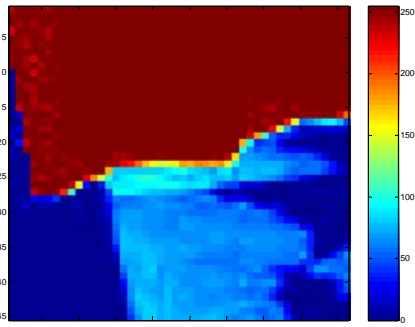Fig 8 QuikSCAT Rain-flag
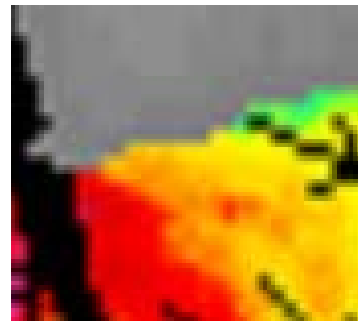


Fig 9   TRMM rain-rate

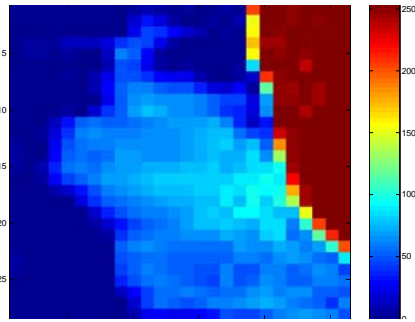Fig. 10 QuikSCAT False Alarms



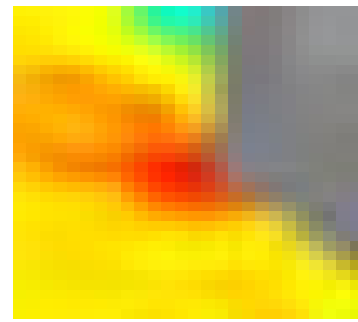Fig. 11 Strong Wind Regions



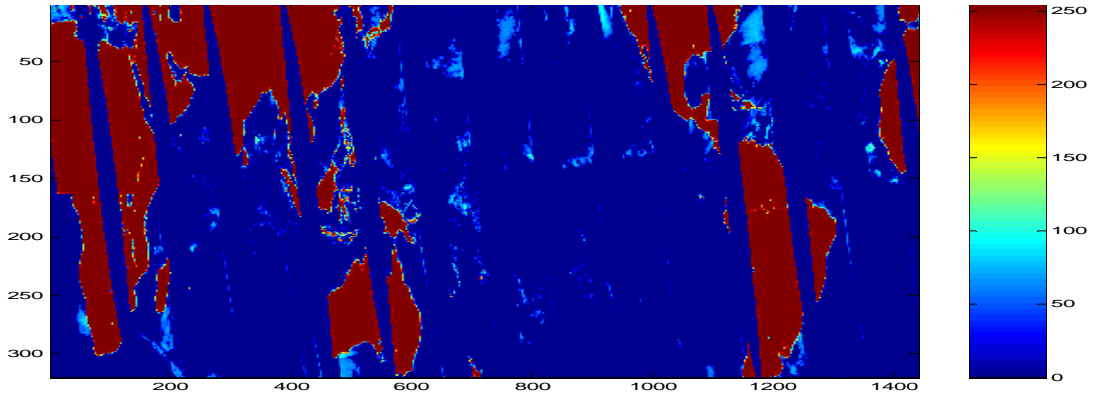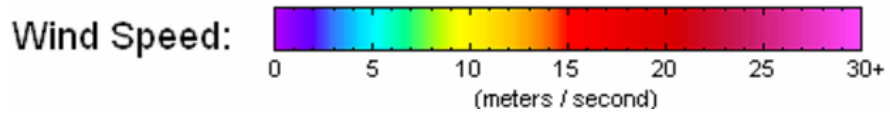Fig.12 QuikSCAT False Alarms



Fig. 13 Strong Wind Regions



Wind Speed:
0   5   10   15   20   25   30+
(meters / second)



Fig. 14 QuikSCAT Rain-Flag using Multi-fractals (Morning Pass)
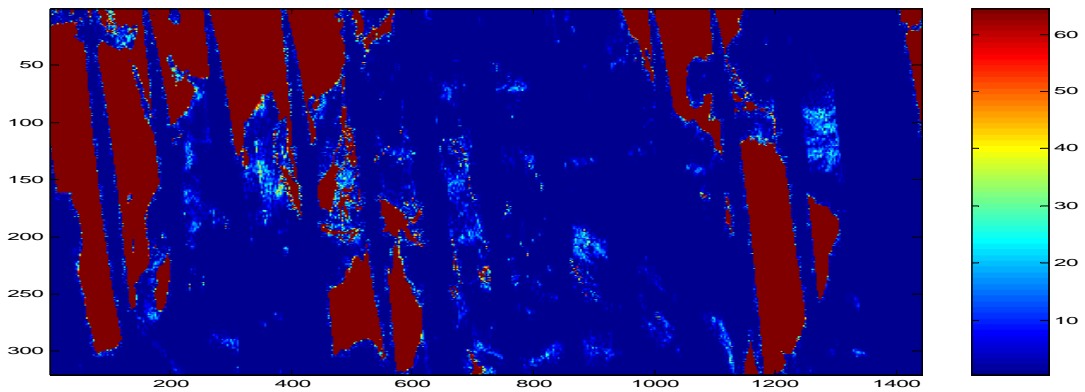


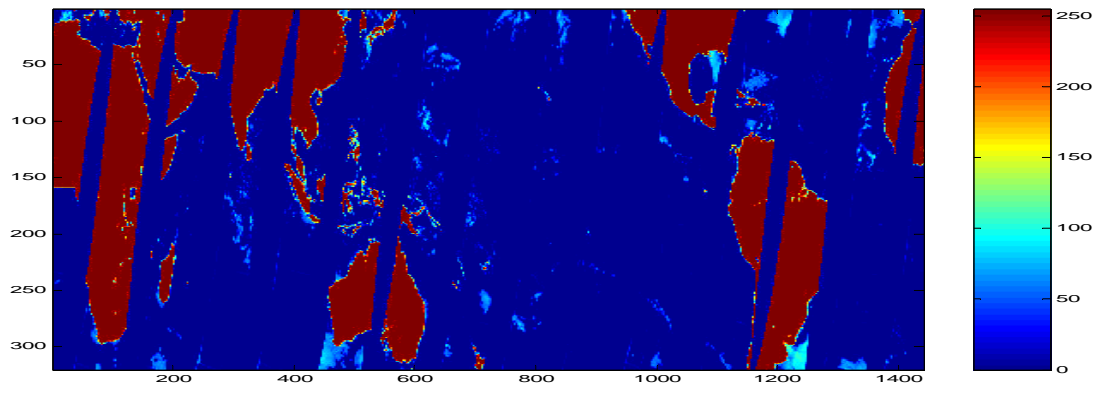Fig. 15 QuikSCAT Rain-Flag using Differential Polarization(Morning Pass)

7
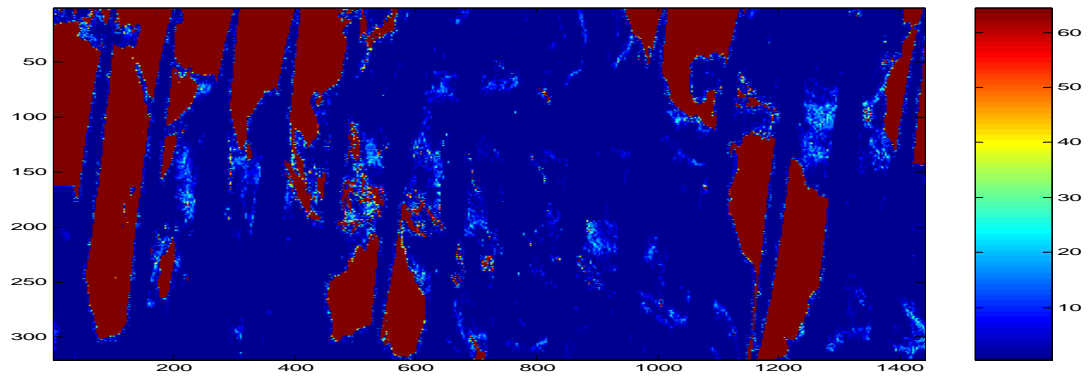
Fig. 16 QuikSCAT Rain-Flag using Multi-fractals (Evening Pass)



Fig. 17 QuikSCAT Rain-Flag using Differential Polarization(Evening Pass)

8